An empirical approach to studying debris flows: Implications for planetary modeling studies

Mark H. Bulmer,[1] Olivier S. Barnouin-Jha,[2] Mathew N. Peitersen,[3] and Mary Bourke[4]

Received 26 June 2001; revised 29 November 2001; accepted 6 December 2001; published 28 May 2002.

[1] High-resolution images acquired by the Mars Global Survey Mars Orbiter Camera show gullies on the walls of impact craters and valley systems on Mars. Depositional aprons associated with these gullies have been interpreted by *Malin and Edgett* [2000] to be characteristic of debris flow and to indicate the presence of sources of liquid water at shallow depths below the Martian surface. By focusing on a terrestrial debris flow we test the application of Chezy-type modeling to provide more direct estimates of the dynamics of proposed debris flows on Mars. Traditionally, planetary scientists, constrained by available remotely sensed data, have used a range of flow models to gain insights from deposits into the behavior and rheologic nature of features such as lava flows, debris flows, and gravity-driven flows. On the basis of these model results, broad interpretations of the physics governing flows of granular materials have been tempting based on limited field-derived data. This study tests and validates the extent to which the absolute value and relative variations of empirical parameters derived from the Chezy-type models describe the behavior of the General's slide debris flow (38.24°N, 78.23°W) in Madison County, Virginia. The results indicate that extreme caution must be taken when interpreting model results for turbulent flows of granular materials. We obtained high-precision topographic profiles, superelevation data, sedimentary facies, and sedimentary textural properties over the debris flow. This study focuses on the empirical parameter C, whose value gauges energy dissipation in a flow, thereby called flow resistance. Using field observations, both variations and absolute values of C along the debris flow have been computed using two approaches: (1) assuming constant volumetric flow rate Q, where only topography and high-resolution images are required to compute channel dimensions, and (2) a variable Q, calculated using field derived data. Assuming near-Newtonian flow conditions in the debris flow, estimated values of C range from 0.035 to 0.099. When Q is fixed, C decreases as a function of distance downstream. When Q varies and C is computed from field-derived flow speeds, its value tends to increase downstream slightly. These opposite results have been compared to the field observations to determine which best describes the behavior of the flow. The variations in C downstream, obtained using the flow speeds, are most consistent with the geomorphic evidence for erosion of material by the debris flow and the presence of bends in the channel. The average values of C, 0.036–0.33 for the General's slide, have been compared with computed C values for Newtonian and near-Newtonian flows to assess the rheology of the flow during emplacement. Our terrestrial study demonstrates that advances in understanding of the dynamics of debris flows on the Mars depends on obtaining debris flow speeds in addition to channel topography and flow thickness, rather than just on channel topography, flow thickness, and the assumption that Q is constant. Mars Orbiter Camera (MOC) and Mars Observer Laser Altimeter (MOLA) data can be used to derive channel topography, flow thickness, and possibly flow speeds. Such data will provide more direct estimates of the dynamics of debris flows on Mars than are currently available. *INDEX TERMS:* 5470 Planetology: Solid Surface Planets: Surface materials and properties; 5494 Planetology: Solid Surface Planets: Instruments and techniques; 6225 Planetology: Solar System Objects: Mars; 8040 Structural Geology: Remote sensing; 8194 Evolution of the Earth: Instruments and techniques; *KEYWORDS:* debris flow, Chezy, modeling, planetary, General's slide, Mars

1. Introduction

[2] The term debris flow is used here to denote a viscous to highly fluid form of rapid mass movement of granular solids, vegetation, water, and air, with flow properties that vary with water content, sediment size, and sorting of particles. Its main driving force is gravity. Four main types of models applied to debris flow deposits provide insights into their flow behavior and rheological nature, which in turn allow better forecasting of debris flow hazards and forward modeling of landscape evolution. These

[1]Joint Center for Earth Systems Technology, University of Maryland, Baltimore County, Baltimore, Maryland, USA.
[2]Johns Hopkins University Applied Physics Laboratory, Laurel, Maryland, USA.
[3]Proxemy Research, Laytonsville, Maryland, USA.
[4]School of Geography and the Environment, University of Oxford, Oxford, UK.

0148-0227/02/2001JE001531$09.00

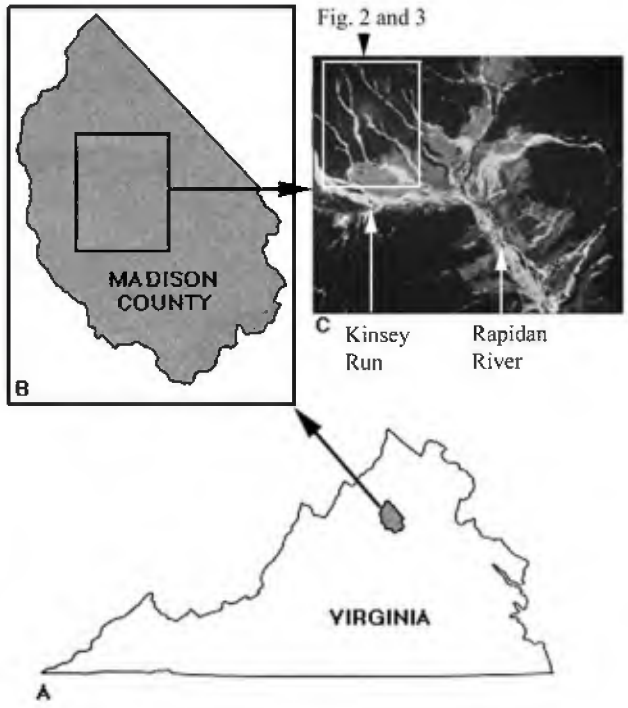

Figure 1. Location map. (a) State of Virginia, (b) Madison County, and (c) an aerial photograph of the area around Graves Mill.

include (1) viscoplastic models [e.g., *Johnson*, 1970, 1984], (2) inertial grain flow models [*Takahashi*, 1980, 1981], (3) fluid-solid momentum transport models [*Iverson*, 1997], and (4) empirical Chezy-type models [*Weir*, 1982].

[3] A simple viscoplastic model considers a debris flow as a single phase Bingham or Coulomb continuum [*Johnson*, 1970]. At low shear stresses this model treats a given debris flow as an elastic solid, which at higher shear stress, flows viscously. The model possesses the advantage that its rheological characteristics as expressed by yield strength, cohesion, and the Bingham viscosity can be derived from field observation [*Johnson*, 1984]. However, such models do not accurately describe the observed motion or deposits of debris flows: they do not take into account either particle-particle or particle-fluid interactions that occur within a debris flow and which significantly influence their motion and deposition [*Iverson*, 1997; *Sohn*, 2000].

[4] In order to account for such particle-particle interactions, *Takahashi* [1980] developed the inertial grain flow model. It builds upon *Bagnold*'s [1954] work that shows changes in the relationship between normal and shear stresses for grains suspended in a fluid of equal density, where these stresses vary either quadratically or linearly with shear rate. The two shear rate regimes, named "grain inertia" and "macroviscous," are determined by the ratio of inertial to viscous shear stress in the suspension. *Takahashi* [1980] used the grain inertia relationship to model debris flows. While his model improves on the viscoplastic model by including the particle-particle interactions, it still possesses limitations. It assumes a uniform distribution of particles in the flow and does not allow the interstitial fluid and matrix mixture to sustain any pressure [*Iverson*, 1997; *Sohn*, 2000]. This is contrary to field observation and recent experiments which show debris flows traveling in a bimodal fashion, with the coarser debris traveling ahead of a more fluid tail that sustains pore pressure [*Iverson*, 1997; *Major and Iverson*, 1999].

[5] Unlike the previous two models, the fluid-solid momentum transport model and the empirical Chezy model have more general applications. Both these models minimize the assumptions made on the physical characteristics of a debris flow. The fluid-solid momentum transport model developed by *Iverson* [1997] generalizes the theory by *Savage and Hutter* [1984] for granular flows to include viscous pore fluid. This model therefore incorporates both fluid-particle and particle-particle interactions and is a good predictor of laboratory-generated, unsteady, nonuniform motions of experimental debris flows [*Iverson*, 1997]. However, this model requires a numerical approach to determine the rheological properties of a debris flow based on field observations of flow heights and velocity. This makes predictions for both debris flow hazards and landscape evolution a time consuming process.

[6] Chezy-type models [*Weir*, 1982; *Baloga et al.*, 1995; *Bruno et al.*, 1996] are empirical in nature. Consequently, they make no prior assumptions on the nature of the debris flow but rather parameterize using constants the momentum transport and energy dissipation of debris flows. While not explicitly describing the physics of a debris flow, these parameters, when properly calibrated, can provide a first-order view into the behavior of debris flows ranging from rock avalanches to sediment laden water floods.

[7] Such Chezy models possess several advantages. The empirical parameters, which may potentially constrain the rheological nature of a debris flow, can be derived from topographic data, airborne or space-based imaging (including thermal and radar), and field data. If the empirical parameters prove to be consistent with detailed field observations and laboratory experiments, they provide excellent constraints for the development and use of more sophisticated debris flow models such as the fluid-solid momentum transport model. These parameters can also be applied directly in simplified momentum equations to assess debris flow hazards and develop landscape evolution models for regions where the behavior of debris flows are well known. Such an approach has been used with success to predict lava flow behavior on the Earth and other terrestrial planets [e.g., *Baloga et al.*, 1995].

[8] This study tests and validates the extent to which the absolute value and relative variations of empirical parameters derived from the Chezy-type models describe the behavior of debris flows. The strengths and limitations of two model versions are established by comparing derived empirical parameters obtained at the General's slide, a debris flow located near Graves Mill in Madison County, Virginia (Figure 1), to a wide array of field data and eyewitness accounts [*Wieczorek et al.*, 1996, 2000; *Morgan et al.*, 1997]. These derived parameters are also compared to similar empirical parameters obtained from other well-documented debris flows as well as other mass movement types. While our goal is to better understand mass movement processes on the terrestrial planets, particularly Mars, we have focused in this study on a terrestrial example taking into account the data constraints imposed on planetary scientists. By first testing our methodology on Earth, we have determined the validity of the approach and that by using dimensional information obtained from Mars Orbiter Camera (MOC) and Mars Observer Laser Altimeter (MOLA) data it will be possible to obtain more direct estimates of the dynamics of debris flows on Mars than are currently available.

[9] This paper is divided into seven sections. section 1 provides some background to the conditions which led to the formation of the General's slide and the type of topographic, photogeologic, geomorphic, and eyewitness data obtained at the field site. We include a brief description of how the topographic data were collected. Sections 2 and 3 describe the geomorphology of the General's slide. Section 4 describes the two Chezy model versions used to derive the empirical constants while analyzing the General's slide. Sections 5 and 6 present and compare the derived

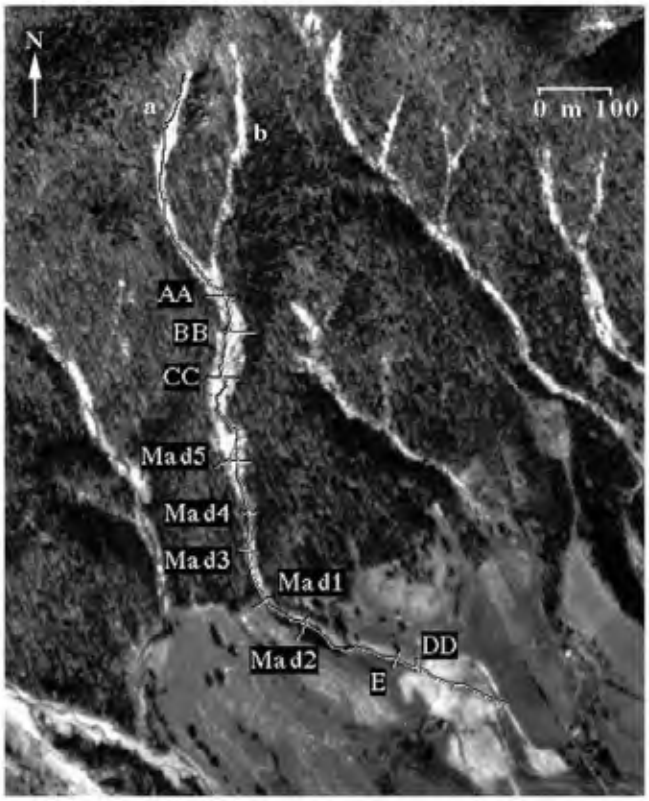

Figure 2. Air photo from 24 March 1997 showing the General's slide from flow source area a and b to the depositional zone DD. Transects carried out both along and across the channel are shown. The letters with black backgrounds refer to individual across channel transects. Image is 1:18,000 scale.

parameters to the observed field data and identical parameters obtained at other field sites. Implications for use of the Chezy models in both terrestrial and planetary studies are presented in section 7.

2. Field Site and Geomorphologic Data Set

[10] Historical debris flows have been reported all along the Appalachian Mountains, and stratigraphic evidence indicates that debris flows have been important geomorphic slope processes throughout the Quaternary [*Mills*, 1982; *Kochel and Johnston*, 1984]. The area containing our study site is prone to debris flows because of steep upper slopes (>20°) and surface weathering which has turned the underlying coherent granitic quartzo-feldspathic bedrock [*Allen*, 1963] into a loose top layer of friable soils with substantial quartz sand and clay. Colluvium formed from soil creep and slope wash overlays some of the steeper slopes (slope >10°). With sufficient rainfall this loose layer mobilizes on the upper steep slopes to form debris flows.

[11] Most recently, an intense storm on 27 June 1995 centered over an area of ~75 km^2 triggered hundreds of such rock, debris, and soil slides from the steep hillsides of the Blue Ridge Mountains [*Wieczorek et al.*, 1996]. Most of these slope failures transformed into debris flows (Figure 1c). During ~16 hours, as much as 770 mm of rain fell in the area of maximum storm intensity, and probably ~640 mm fell within a 5 hour period over small areas [*Wieczorek et al.*, 1996].

[12] We have investigated the "General's slide" debris flow originating from the 1995 storm. The debris flow is located close to Graves Mill in Madison County, Virginia (Figure 2). We collected a large range of geomorphic data. These include (1) high-resolution GPS topography both along and across the channel, including superelevation data at various bends in the channel, (2) extensive geomorphic descriptions of the channel pertinent to the debris flow(s), (3) sedimentary profiles along the channel, (4) sedimentary analysis of matrix and boulders comprising the debris flow deposits and located along the stream channel, and (5) cohesion, internal friction, and permeability of the soil at the debris flow's source. These data are complemented by a wealth of regional photogeologic, sedimentary, and geomorphological data as well as eyewitness accounts obtained by the U.S. Geological Survey [*Wieczorek et al.*, 1996, 2000; *Morgan et al.*, 1997]. This study uses primarily the topographic data and geomorphological description along with the sedimentary profiles.

[13] Field data collection was designed to characterize channel topography, surface roughness, and dimensions of the General's slide debris flow to derive the necessary inputs to test the Chezy models. Profiles along and across the channel were used to determine slope, surface roughness, and cross-sectional surface as well as flow depths and speed. The main channel of the General's slide was surveyed (Figures 2 and 3) using a Trimble Total Station 4800, which consists of two GPS receivers that work in tandem. This equipment uses carrier phase differential processing for 1 cm horizontal real-time accuracy. One receiver remains fixed on a tripod at a known location during the survey. The location of this receiver was determined to an accuracy of 1–2 m using a Trimble ProXRS GPS unit with satellite-based differential correction. This base station was then used as the reference point for all subsequent surveys. The roving Trimble 4800 receiver used

Figure 3. Anaglyph of 1:18,000 scale air photographs from April 1991 (right eye) and March 1997 (left eye) showing the landscape change between these dates resulting from the storm in July 1995 (orange coloration). The image in the left eye shows the area around the General's slide two years after the 1995 storm. Compare this to the image in the right eye that shows the area of the General's slide as it was in 1991. The channel was tree covered and is shown by the blue colored transect lines seen in Figure 3. Comparison of the debris apron with Figure 2 taken August 1995 shows that much of the material in the depositional zone has been removed by heavy machinery to restore the productivity of the field. See color version of this figure at back of this issue.

for data collection is mounted on a pole 1.8 m in length. This pole allows the survey team to determine positions even in the small spaces between megaclasts, so the topography can be adequately characterized. A radio link, provided by a 25 W UHF radio at the base station, is constantly maintained for real-time differential correction. While conducting transects up the main channel, a three-dimensional (3-D) point was collected approximately every 3 m. This spacing was determined in the field to adequately represent the topographic character of the channel profile and to meet the resolution requirements of the empirical model. For the transect up the channel (transect 1) we obtained 1 cm horizontal and 2 cm vertical accuracy per point (relative to the base station) to ~1000 m up from the lower end of the debris flow. Beyond that point we encountered difficulties in satellite coverage (<4 seen) due to screening by the tree canopy reducing the accuracy to 20–40 cm. We successfully collected data up to the top of the main channel, covering a transect distance of 1600 m.

[14] In addition to the main channel transect we also measured 10 cross-channel profiles (Figure 2) using a laser rangefinder (Laser Atlanta Advantage CL) connected to the Trimble ProXRS. A 3-D point was collected every 3–6 m with an accuracy of 10–15 cm. The position of each cross-channel profile relative to the main channel was determined to an accuracy of ~1 m by locating points that had been surveyed previously using the Trimble 4800. The cross-channel transects were taken where a measurement of depth for the 1995 event could be determined and we could identify the location on air photos. Geomorphic signatures of the 1995 event that we used to determine debris flow depths included locations where tree, soil, and rock had been pushed up against the base of tree trunks on the channel banks and on the edge of the channel. These marks are referred to as trimlines. Such information was also used to determine the extent of debris superelevation in channel bends. Superelevation is the amount by which the outer side of a curved flow is elevated above the inner side of the flow to counteract the effect of the centrifugal force of the flow. Measurements of minimum depths were also collected where fines from the 1995 event had been deposited on top of large boulders. At some locations (transects Mad5 and Mad4) it was difficult to determine the edge of the 1995 event. At these locations we extended the profile out to the first available geomorphic indicator of ground that was undisturbed by the 1995 event. Using this procedure, we attempted to obtain the maximum possible width measurements.

3. Geomorphologic Description

[15] Geomorphic evidence indicates that more than one pulse formed the General's slide debris flow deposits and that they were likely transitional between hyperconcentrated flow and debris flow. A hyperconcentrated flow is a mixture of flowing water and sediment (40–80% sediment load by weight) that has a yield strength but still appears to flow like a liquid. No one saw the debris flow(s) in the General's channel, but at least three people witnessed others in the immediate area. Randall Lillard, whose farm is in Graves Mill ~2 km from the General's slide, made a video recording of parts of the storm and other debris flows that damaged his house. From this point on, the discussion of the General's slide focuses on the main debris flow event on 27 June 1995, rather than individual pulses, the geomorphic signature of which were altered and overprinted by successive events.

3.1. Air Photo and Field Interpretation

[16] Well-delineated stream channels and new deposits in the grazing land resulting from the 27 June 1995 storm are clearly shown on air photos taken in March 1997. Comparing these photos with those taken in April 1991, significant changes can be recognized (Figure 3). (1) Prior to the storm of 27 June 1995, the drainage course(s) on the wooded slopes of the General's slide are not visible. After the storm, the streamlines of the General's slide are

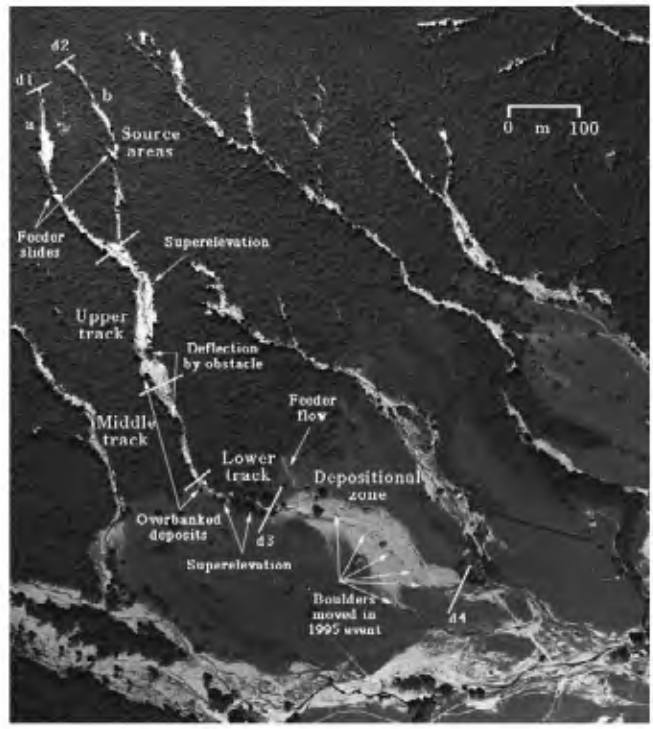

Figure 4. Subscene from 1:18,000 scale air photo of the Graves Mill area, taken 22 August 1995 showing the General's slide several months after the debris flow event. The depositional fan of General's slide is clearly evident. Examples of geomorphic features such as overbanking and superelevation are labeled.

clear, as indicated by orange/red tones. (2) A large part of the tree, vegetation, and soil cover in the drainage channels and on the edge of the channel was swept away, exposing bedrock. (3) A high trimline on both sides of the General's stream indicates the level that the debris flow reached during movement. (4) A small ridge was locally overtopped between CC and Mad5 (Figure 2). (5) Superelevation sites can be recognized on both sides of the channel. (6) The debris flow overtopped the channel in the lower reaches and left deposits on the down flow right side before becoming unconfined upon emergence on to grazing land. (7) The debris flow spread laterally over the field and deposited clasts ranging from clay to blocks (13 to -13Φ). In the air photos from 1991 it is possible to see that some boulders and blocks already existed at the channel mouth. Some of these were moved and overtopped by the 1995 deposits. (8) The debris flow then entered the mainstream from Kinsey Run, which flows into the Rapidan River.

[17] Interpretation of photographs from August 1995 (Figure 4) is that the 1995 event began as rock/debris slides at the heads, "a" and "b" of the General's stream. The timings of failure are unknown. Once in motion, the rock/debris mass descended down the narrow and steep (45°–30°) channels growing in volume with the inclusion of water, rock, soil, and vegetation. It entered the main channel at AA (Figure 2) and impacted the downstream left side of the channel between BB and CC, knocked down trees, and dislodged boulders. The debris flow was confined to the channel downstream of CC until some portion overtopped the small ridge (downstream right bank) on the bend above Mad5 (Figures 2 and 4). The main flow continued down the channel stripping trees, soil, rock, and vegetation. At Mad5, there are large boulders in the channel, and there is evidence that parts of the flow went out to the downstream right bank of the channel at this point. It rejoined the main flow below Mad5. Below Mad5 to Mad1 the main part of the debris flow was confined to a preexisting channel with a bedrock floor and sides. The flow

Figure 5. View of the source area d1 in channel a of the General's slide.

overtopped this section of the channel but did not topple trees, instead leaving high-water lines on their trunks. At Mad1 the channel is deflected by an ancient alluvial fan. Here the debris flow impacted the downstream right bank (Mad2) and apparently plucked clasts from the exposed alluvium. Below Mad2 the channel walls are composed of weak highly weathered granite that was eroded and included into the flow. Beyond the tree line the debris flow emerged from the channel carrying a range of coarse sediment sizes, trees, and soils. Virtually all tree trunks were debarked and stripped. The flow spread out over the field, depositing boulders and blocks near the center of the streamline.

[18] Measured on the air photo (August 1995), the distance from the top of channel a (d1) of the General's slide to the edge of the tree line (d3) is 919 m, and from the top of channel b (d2) to the same location (d3) is 925 m (Figure 4). The elevation change over this length is 329 m. The main deposit (d3 to d4) is 311 m long and 93 m at its widest, w (Figure 1). It covered an area 0.02 km^2. Eyewitness accounts estimate the thickness t of the deposits to have been ~1 m. Using l, w, and t, we have derived a first-order volume estimate of 21,960 m^3 of deposited material. This is significantly greater than that which could have been derived solely from the source areas a and b, whose maximum combined first-order volumes based on an average w and t measured at the scarp (a = 1 m and b = 0.4 m) equals 5244 m^3. This supports our inference that a significant volume of material was eroded and incorporated into the flow from along the length of the channel.

3.2. Field Observations of the General's Slide

3.2.1. Source areas. [19] At the source areas the drainage channels a and b are V shaped, and the slopes are steep. The locations of the scarps d1 and d2 identified in the field matched closely those in the 1995 air photos. On the basis of that observation we suggest that little postmodification had occurred at the scarps. At a the scarp is 14.7 m wide and 0.7–1.0 m deep and occurs on a 48° slope (Figures 4 and 5). The distance from the scarp to the confluence above AA is 388 m. The width of the channel ranges from 3 to 17 m. We calculate a first-order volume using w = 10.5 m and t = 1 m of 4074 m^3. Channel b is similar in nature to that at a. The scarp at d2 is 8.4 m wide and 0.4 m deep and occurs on 56° slope. The distance from the scarp to the confluence above AA is 424 m. The width ranges between 3 and 10 m. We calculate a first-order volume using w = 6.9 m and t = 0.4 m of 1170 m^3. The thin soil layer overlying the bedrock controls the shallow depth of the failure. The soil coverage is mainly a shallow, clay-rich soil derived from the weathered bedrock with a well-developed, permeable uppermost horizon. The bedrock provides an impermeable layer to water, which then flows downslope under the soil layer. During the prolonged wet period in the days prior to the storm on the 27 June the soils became saturated, causing strength reduction. The initial failures at d1 and d2 appear to have been shallow translational soil and rock slides which transitioned to debris flows as they descended.

[20] The channels are filled with loose pebbles and boulders of weathered bedrock (Figure 6) and appear to fit the weathering-limited classification of *Bovis and Jakob* [1999]. This loose material is easily set in motion on the steep slopes. Downstream in channel a, there is at least one other slope failure that is 17 m long and 8.7 m wide (maximum) and ranges from 0.7 to 2.4 m in depth. To first order, this failure contributed 283 m^3 of soil to the channel. Downslope, the channel walls consist of exposed solifluction materials, which provide a ready source of clasts ranging from pebbles to small boulders.

3.2.2. Upper track. [21] The two channels, a and b, coalesce into one main channel at AA (Figure 2). Superposition relations show that materials from channel a lie on those from b, indicating that they were deposited from one of the last pulses of material to

Figure 6. View up channel a to the head scarp at d1. Note the boulders in the channel and an example of a feeder flow on the left side of the image.

Figure 7. View up the channel from Mad5 to AA where a and b enter the main channel. The flow stripped the trees and vegetation from the channel sides and became superelevated on the downstream left side shown here in the right of the image.

descend. On either side of the channel immediately below AA, there are boulders (>3 m in length) aligned along the edge. Those on the downstream right side appear to have been emplaced prior to the 1995 event and were not touched by the 1995 debris flow. Boulders on the left side were overtopped, have percussion marks, and in several cases were rotated. Between AA and Mad5 the channel was stripped, and bedrock was exposed (Figure 7) by the debris flow. The majority of leaf litter and trees from the downstream left side was removed and carried away. Only a small part of the flow overtopped the right side, where the channel bends below CC. Where overbanking occurred, there are several boulders. Downstream from this bend the channel becomes more V shaped and contains at least three large blocks (9–10 m in length). These blocks appear to have been in the channel prior to the 1995 event and have coarse clasts deposited on them as well as percussion marks. The height of one of these blocks is at least 8 m. Part of the flow was divided around a large block and a logjam, rejoining the main flow at Mad5.

3.2.3. Middle track. [22] Between Mad5 and Mad4 the channel opens out and was crossed by a jeep track. There are several large boulders against standing trees. These boulders were moved there during the 1995 event and appear to have been at the flow margin (Figure 8). The velocity of the flow was not sufficiently high to knock the trees over, but they are leaning, presumably due to the boulders being pushed against them by the flow. At Mad4, there is a break in slope in the channel caused by at least seven large granite boulders (Figure 9). The timing of emplacement of these boulders is unknown, but they show percussion marks from the 1995 debris flow, and there is matrix around and between them. Weathering patterns on them show they were moved on their axis during the 1995 event. There is evidence that a part of the flow went around the down flow right side of the main channel following a small preexisting drainage line before rejoining the main channel above Mad3 (Figure 4). Where this

Figure 8. Example of a boulder pushed against a tree by the 1995 flow situated on the downstream left side of the channel ~10 m upstream of Mad4.

Figure 9. Large boulders that fill the channel at Mad4. Percussion marks from the 1995 debris flow, weathering surfaces, and the range of materials surrounding the boulders can be seen.

Figure 10. A view looking downstream of a sheared tree trunk with clasts from the 1995 debris flow embedded in it. The tree is situated on the downstream right side of the channel between Mad4 and Mad3.

happened, the flow had sufficient momentum to knock down trees but also deposited pebble-sized clasts. Figure 10 shows clasts from the 1995 flow embedded in the trunk of a fallen tree situated on the down flow right side of the main channel between Mad4 and Mad3. One interpretation of the geomorphology at Mad4 is that the channel may have become temporarily constricted as trees became trapped against the boulders, causing part of the flow to go round to the right. Alternatively, the flow may have spread laterally after Mad5, as a response to the wider channel and lower gradient slope, causing part of the flow to travel to the downstream right side of the boulders at Mad4. While this occurred the main part of the flow had enough momentum to overtop the boulders at Mad4, causing the observed percussion strikes. The main channel below Mad4 to Mad1 has bedrock walls and floor. There are no boulders, blocks, or tree trunks in this section of the channel. There are mud splatter marks, tree trunk rubbings, and materials wrapped around trees, which all give an indication of the flow depth. The average depth to the channel floor is ~5 m.

3.2.4. Lower track. [23] Just above Mad1 the character of the channel changes from coherent bedrock to heavily weathered granite and colluvium (Figure 11). The channel is forced to make a turn to the left because of the presence of a paleofan. At Mad1, there is evidence for overbanking on the down flow right side with matrix deposited on the paleofan surface (Figures 4 and 12). On the down flow left side, tree trunk rubbings at Mad1 indicate a flow depth of 4.5 m. The right bank of the channel exposes the paleofan, and the 1995 event appears to have been erosional, incorporating fan materials into the flow(s). The present channel narrows at Mad2, becoming V shaped, and then widens upon reaching the open field above E. There is evidence for superelevation and overbanking at Mad2. Mud spatter marks and tree trunk rubbings indicate that the flow on the down flow right side was ~3 m higher than at the down flow left side.

3.2.5. Deposition zone. [24] Between E and DD (Figure 2), there is a large number of boulders and blocks which range up to >10 m in diameter (Figure 13). Some are aligned along the downstream left side of the channel and were emplaced prior to 1995. These were overtopped by the 1995 flow and in some places moved. Many of these megaclasts show percussion marks and exposed weathering lines. Some boulders and blocks were carried beyond DD (Figure 4). The deposits consist of matrix-supported clasts and macro-organics with a range of sediment sizes from blocks to clay.

3.3. Debris Flow Deposits

[25] The debris flow deposits are best seen in the depositional zone, although 0.1–0.2 m thick patches of debris flow deposits are preserved throughout the length of the channel. The debris flow event is remarkable for the number and size (Figure 13) of boulders and blocks that were entrained and deposited. One of the largest megaclasts in the channel (Figures 6 and 13) is 3.10 m in length. Boulders and blocks from the basement coherent granitic quartzo-feldspathic bedrock are easily distinguished and were produced during colder climate phases. We suggest these were transported in pulses downslope during infrequent prior events. Most large boulders and blocks were remobilized during the 1995 event or acted as major obstacles to the flow. Forty-five per cent of boulders and blocks have evidence of breakage or removal of weathering rinds, and the majority (83%) are in the subrounded to subangular categories. We propose that the majority of the boulders and blocks in the depositional zone were entrained from earlier depositional sequences in the channel.

[26] The grain size distribution of the matrix of the 1995 event was determined by three methods: field measurements of coarse sediments, wet sieving −4.2 to 4.0Φ pebbles to coarse silt, and use of a Coulter counter <4.0Φ. Results from locations from the source to the depositional apron are shown in Figures 14 and 15

Figure 11. View looking up the channel from Mad1 to Mad3. The transition from bedrock-controlled channel floor and sides to the colluvium surface is apparent. The photo is taken standing on the paleofan.

Figure 12. View looking down the channel from Mad1 to Mad2 taken in 1999. Boulders can be seen in the channel as well as the evidence for overbanking and superelevation on the downstream right side.

Figure 13. View across the part of the depositional zone at DD taken in September 1995. Note the range of material sizes. Percussion marks and weathering surfaces can be observed on the boulders. Some alignment of the boulders down flow is also apparent. A boulder identified in the 1991 air photos and therefore predates the 1995 debris flow can be seen in the left of the image in the midground.

using the modified Udden-Wentworth grain size scale [*Blair and McPherson*, 1999]. As expected, the debris flow matrix supporting the boulders and blocks is poorly sorted and displays a large range in the percentage silt and clay content (Figure 14). This range has no clear relationship with either the depositional environment or distance down flow.

4. Chezy Model

[27] The empirical Chezy model has been used successfully to describe a wide range of quasi-Newtonian and Newtonian flows, including river and open-channel flows [e.g., *White*, 1993], lahars [*Weir*, 1982], lava flows [e.g., *Baloga et al.*, 1995, 1998; *Bruno et al.*, 1996], turbidity flows [e.g., *Simpson*, 1997], and sediment-laden flows [e.g., *Komar*, 1980]. Use of such a model assumes (1) one-dimensional flow at any point along a flow where the velocity in the flow is averaged to a single value u and (2) no significant density variations in the fluid. A typical version of the Chezy model is given by

$$Q = uA = (gh \sin \theta / C)^{0.5} A, \quad (1)$$

where Q is the volumetric flow rate, A is the cross-sectional area of the flow, g is gravity, θ is the underlying slope, h is an average flow thickness, and C is empirically derived. This Chezy equation describes the volumetric flow rate at any instant of time where measurements for A, h, Q, and C are available. The average weighted flow thickness $h = A/w$, where w is the width of the flow. In the hydraulic literature [e.g., *White*, 1993], $h = A/P$ and is defined as the hydraulic radius, where P is the wetted perimeter of the flow, which includes the sides and bottom of the channel but not the upper free surface. In this study, we will not use the latter definition because the differences between the wetted perimeter of the flow and its width are small, thereby not significantly altering the final outcome of this study.

[28] This study focuses primarily on the empirical parameter C, whose value gauges the energy dissipation in the flow. As defined in (1), C is the effective resistance to the down slope motion of the flow by gravity, thereby called flow resistance. This study computes both variations in and the absolute value of flow resistance along the General's slide and establishes whether these are consistent with our field interpretation of the slide's flow dynamics.

[29] We take two approaches to estimate the changes in C downstream. First, we assume that there is no change in the volumetric flow rate Q along the General's slide. This assumption minimizes the amount of data required to understand the flow dynamics of a debris flow when using (1). Only topography and high-resolution imaging are required to compute the channel dimensions as expressed by h and A. This approach allows determination of the behavior of the debris flow downstream only in relative terms and makes it difficult to accurately constrain the rheology of the flow.

[30] The second approach relaxes the condition that Q must be constant. In this case, additional information (flow speeds based on observed superelevation) is used to determine the changes in C downstream. An alternative approach [e.g., *Baloga et al.*, 1995; *Bruno et al.*, 1996] solves simplified momentum equations for the debris flow and uses average flow thickness rather than velocity to constrain C. In addition to determining the actual changes in C downstream, both of these methods possess the advantage over the constant Q approach that the actual value of C can be estimated. This value can be compared to values of C for other styles of well-documented debris flows, thereby constraining the rheology of the debris flow at the General's slide. The derived rheology was compared to eyewitness descriptions and video data of nearby flows for confirmation.

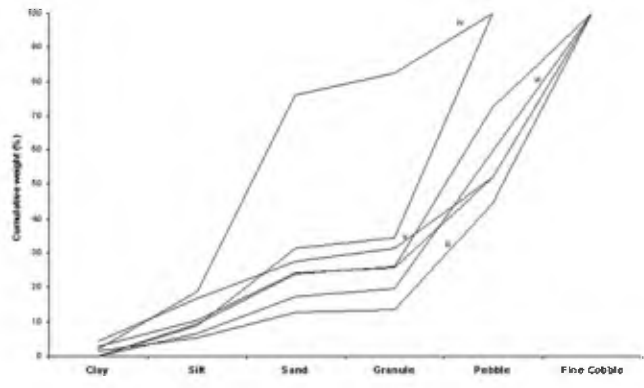

Figure 14. Cumulative weight (%) curves for seven samples from the 1995 debris flow matrix. The silt-clay content ranges between 7 and 19%. Locations i and ii are taken at d1 the top of channel a, iii and iv are from Mad 4, v is from Mad 3, vi is from E, and vii is from the middle of the depositional zone.

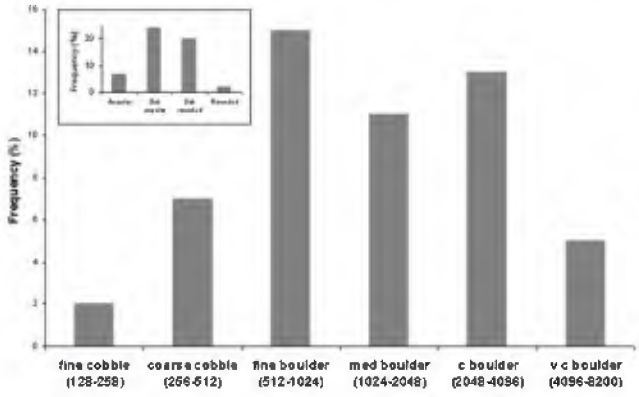

Figure 15. Intermediate length axis (mm) of boulders in the depositional zone classified using modified Udden-Wentworth grain size scale [*Blair and McPherson*, 1999] $n = 53$. Population was measured after some of the larger blocks were removed/buried by remedial works. The long axis of the largest block moved by the 1995 debris flow was 11 m.

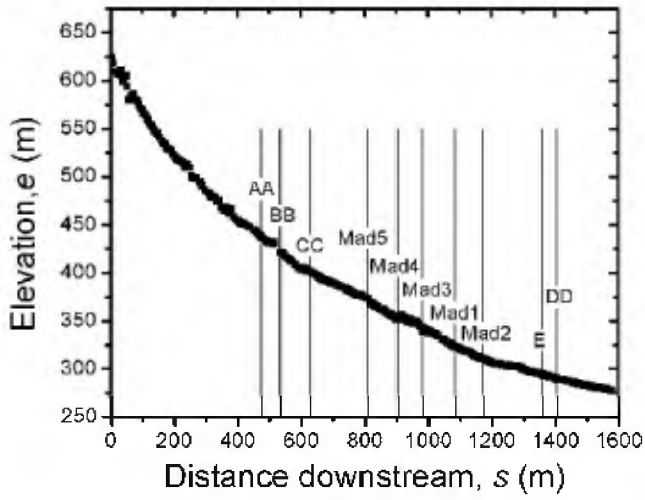

Figure 16. Elevation e of the main channel as function of distance downstream s. Note that there is some roughness (see Figure 17) in channel, with jumps of up to 10–15 m.

4.1. Constant Volumetric Flow Rate

[31] In this first approach, relative changes in flow resistance along a debris flow are easily determined from (1) and the assumption that Q is constant. The value of C at any point n along a flow (henceforth C_n) relative to a value of C at reference point 0 (henceforth C_0) is given by

$$C_n/C_0 = (A_n/A_0)^2[(h_n \sin \theta_n)/(h_0 \sin \theta_0)], \quad (2)$$

where A_n and A_0 are the cross-sectional area of the flow at n and 0, h_n and h_0 are the average flow thicknesses at n and 0, and θ_n and θ_0 are the underlying slopes at n and 0.

4.2. Relaxing the Condition Q as Constant

[32] In this second approach, we use observed superelevation of the General's slide in bends along the channel to estimate its average debris flow speeds at several locations along the channel. The absolute value of flow resistance C at each bend is determined by rewriting (1):

$$C = (gh \sin \theta)/u^2 \quad (3)$$

4.3. Use of Topographic and Geomorphic Data to Estimate θ, A, h, and u

[33] Reasonable flow resistance estimates of a debris flow depend on careful consideration of topographic and geomorphic data obtained in the field. The following section details the assumptions and the method used to determine slope along the channel, the cross-sectional area of the General's slide, its average thickness, and its velocity.

[34] This study implicitly assumes that any flow resistance computed using (2) and (3) is for the largest debris flow pulse that made its way down the General's channel. This assumption results from using the highest watermarks and trimlines visible in the field to define the General's slide debris flow dimensions. As described in section 3, the smaller pulses could not be readily distinguished from the main flow pulse that must have passed through the channel.

[35] In order to determine slope along the General's slide we collected surface topography as described in section 2.1. The main channel's elevation as a function of distance downstream (Figures 16 and 17) indicates the presence of small-scale roughness of at most 15 m, especially near the beginning of the channel. Such roughness could potentially influence the dynamics of the flow. However, several lines of evidence, not least that the debris flow carried megaclasts only slightly smaller than this roughness, show that the debris flow moved at high speeds and was extremely dynamic, particularly below AA where flow resistance is calculated. The inertia of the flow therefore far exceeded any changes in momentum that the observed roughness could have imposed on the flow. This justifies fitting a smooth third-order polynomial to the observed topography (see Table 1) and then taking its derivative to determine channel slope. The relatively high precision of the polynomial fits is further justification for substituting modeled slopes in place of field values. In addition, the resultant curves indicate that the channel profile is in grade (just capable of maintaining a balance between erosion, transport, and erosion), thus implying that the stream has adapted to a local base level and that the 1995 event did not substantially modify the large-scale topography. We are thus justified in using the current postevent slopes in place of the admittedly preferable

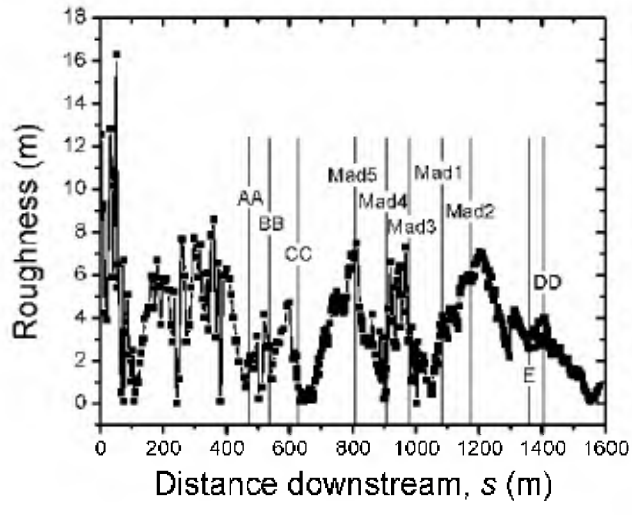

Figure 17. Channel roughness as a function of distance s downstream. Channel roughness was determined by detrending the measured elevation e in Figure 16 with a least squares third-order polynomial fit of e as s (see Table 1) used to compute slope (see text).

Table 1. General's Slide Debris Flow Dimensions

Cross Profile	Downstream Position s, m	Elevation e, m	Slope θ,[a] deg	Width w, m	Depth h, m	Cross-Sectional Area A, m^2
AA	473	438	15.2	49.02	3.81	186.6
BB	535	421	14.1	41.41	3.07	127.1
CC	627	402	12.5	53.61	3.05	163.3
Mad5	808	374	9.9	66.10	1.91	126.4
Mad4	905	352	8.8	21.54	2.77	59.6
Mad3	981	344	8.0	37.01	4.54	167.9
Mad1	1084	323	7.1	34.72	2.53	87.68
Mad2	1173	311	6.5	39.84	4.15	165.2
E	1361	294	5.8	18.69	2.82	52.8
DD	1404	290	5.7	24.28	3.04	77.0

[a] Used third-order polynomial least squares fit of elevation e to calculate slope θ, where $e = 5.6717 \times 10^{-8}\, s^3 + 0.0002544\, s^2 - 0.472968 s + 613.03$, with the standard deviation $\sigma = 2.2$ m.

preevent slopes. Furthermore the well-graded nature of the stream following a major debris flow suggests that such processes have played a dominant role in the development of the channel and maybe more common than previously believed [*Morgan et al.*, 1997].

[36] Both the cross-sectional surface area A and average weighted flow thickness h were determined from cross-channel profiles acquired as described in section 2. The profile obtained at Mad2 is shown in Figure 18 to illustrate the methodology. In order to determine the correct flow dimensions, we first identify high water locations b_1 and b_2 on the channel banks. The area A was then determined by integrating between the straight line linking b_1 and b_2 and the channel floor. The depth h is given by $h = A/w$, where w is the width of the channel from b_1 and b_2. Values for A, w, and h at the 10 cross-channel profiles measured are shown in Table 1.

[37] In order to determine the flow speed, we measured the superelevation of debris flow at bends (e.g., Figure 18). This superelevation can be used to estimate the average flow speed at these bends from the formulation [*Costa*, 1984]:

$$u = [kgR_c(\Delta e/w)]^{0.5}, \tag{4}$$

where R_c is the centerline radius of curvature of the channel followed by the debris flow, Δe is the difference in elevation between the debris flow deposits seen on the two banks of the channel, and k is a constant. The centerline radius of curvature was determined by combining observed geomorphology at bends in the main channel with reasonable second- and third-order polynomial fits $f(x)$ of these bends at the cross transect. The fits were obtained in an x-y plane perpendicular to elevation e. Several possible polynomial fits were considered for those bends where some question arose in defining the actual centerline of the channel taken by the debris flow. The radii of curvature were determined at the intersection of the various fits f(x) with the cross transects using

$$R_c = [1 + (dy/dx)^2]^{3/2} / \left| d^2y/dx^2 \right| \tag{5}$$

where $y = f(x)$.

[38] Many debris flow studies typically use a superelevation $k = 1$ [e.g., *Costa*, 1984], which strictly applies to water. *Mizuyama and Uehara* [1981] suggest that $k = 0.5$, which is empirically valid for water but tends to overestimate the average flow speed in most debris flows, while $k = 0.1$ gives reasonable values for steep slopes of 16° (see discussion by *Chen* [1987]). In estimating flow speed, we use all three values of k, although the most reasonable results are probably bound by $0.1 < k < 0.5$, with wetter debris flows

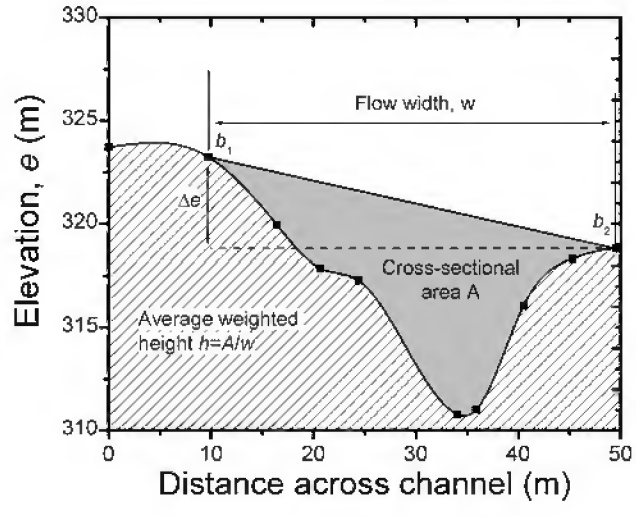

Figure 18. Cross profile obtained at Mad2 illustrating how the cross-sectional area A, the channel width w, the average weighted height h, and the change in elevation Δe are estimated. The direction of flow is toward the reader.

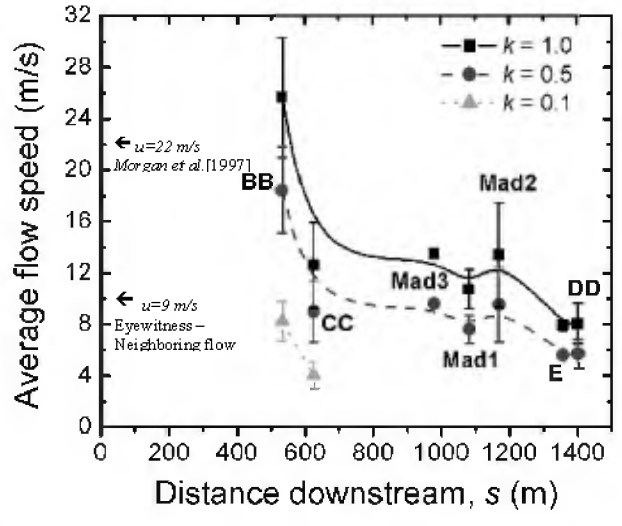

Figure 19. Average velocity of the General's slide at locations along the main channel where superelevation was observed. The three lines correspond to computations of flow speed using three different values for the constant k to determine average flow speed (see text).

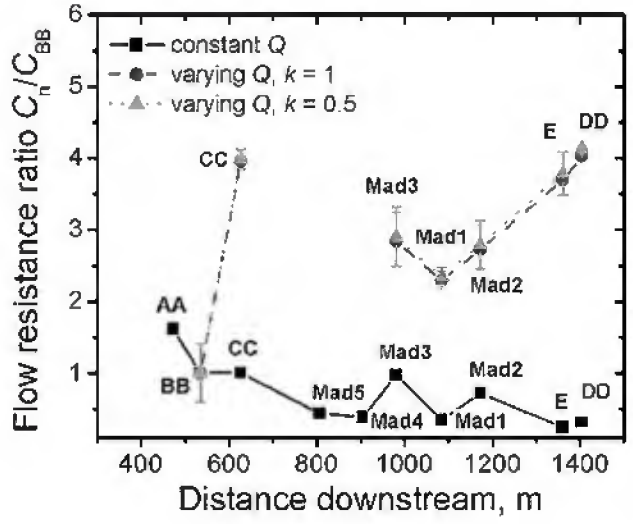

Figure 20. Variations in resistance to flow. All results are referenced to measurements obtained at BB (Figure 3). The solid line is for the case where Q is constant; the other two lines are for when Q is varied downstream. These two latter lines are the result of using two different values for k to determine flow speed from superelevation (see text). The error bars result from the range of flow speeds obtained using different fits for the centerline radius of curvature of the channel.

approaching $k = 0.5$. We only compute flow speed using $k = 0.1$ for the steepest portions of the flow where $\theta > 14.0°$.

[39] Figure 19 shows the flow speed estimates obtained. Some estimates possess error bars that indicate the range of flow speeds obtained by using two or more fits of the channel centerline. The flow speeds obtained are consistent with those of *Morgan et al.* [1997] in the upper portions of the channel and eyewitness accounts near the deposition zone for some neighboring debris flows [*Wieczorek et al.*, 1996; *Morgan et al.*, 1997]. The results for $k = 0.5$ seems to bound the velocity observed by the eyewitness, confirming our suspicion that debris flow speeds are best modeled with $0.1 < k < 0.5$.

5. Model Results

[40] Variations in flow resistance C are shown in Figure 20 for both modeling approaches, where the volumetric flow rate is either held constant or allowed to vary. We choose the cross-channel profile at BB as our reference point (i.e., $C_0 = C_{BB}$). The results show a distinct difference in the behavior of flow resistance between the two modeling approaches. When Q is held fixed, the flow resistance steadily decreases as a function of distance downstream. By calculating the Pearson product moment correlation coefficient this decrease has been proven to be statistically significant. On the other hand, when Q is allowed to vary and flow resistance is computed from the estimated flow speeds, C tends to increase downstream, particularly between BB and CC and Mad3 and DD, as Q decreases over the length of the stream (Figure 21). Using the same statistical technique as for constant Q, the increase in C values below Mad3 is proven to be statistically significant. Between CC and Mad3, there appears to be a slight decrease in C, reflecting a possible change in flow behavior.

[41] Table 2 shows the absolute value of C computed from the estimated flow speeds. These range on average from 0.035 to 0.29. The lowest values correspond to the superelevation flow speeds given by $k = 1$, while the highest are given by $k = 0.1$. We favor values for C bound by $k = 0.5$ that range from 0.023 to 0.0929 since these bound the velocity observed by eyewitnesses for nearby contemporaneous debris flows.

6. Comparing Empirical Theory to Observed Geomorphology

[42] Flow behavior will have influenced the depositional and erosional signature of the General's slide and is a strong function of flow resistance C. As a result, field observations can be used to distinguish between decreasing C for constant Q from increasing C for decreasing Q. In addition, the rheology of the General's slide can be constrained by comparing the computed value of C with other types of quasi-Newtonian and Newtonian flows. Such rheological constraints can be compared with video observations of a nearby debris flow. In section 6.1 we first compare our results for variations in flow resistance with field observations to distinguish between the two model approaches to determine which is most appropriate in describing the General's slide behavior. Second, we attempt to establish and test the rheological nature of the General's slide.

6.1. Distinguishing Between Empirical Modeling Approaches

[43] Factors such as changes in geology and channel shape influence flow resistance during emplacement regardless of modeling approach. However, changes in flow resistance due to changes from laminar to turbulent flow regimes must be excluded. Given the relatively high flow speeds and the size of materials carried by General's slide, it is safe to assume that like many open channel flows, this debris flow was completely turbulent.

[44] The calculated decrease in flow resistance for a constant Q therefore can be the result of four other factors. First, its decrease could simply be the result of decreasing slope downstream. Given that the weighted height h of the debris flow does not change significantly downstream (Table 2), a decrease in slope should result in a decrease in flow speed. In a turbulent flow, such a decrease in flow speed could accompany a decrease in flow resistance. This explanation, however, is unsatisfactory because the effects of slope are already accounted for by (2). In fact, (2) predicts for nearly constant h that the computed decrease in C

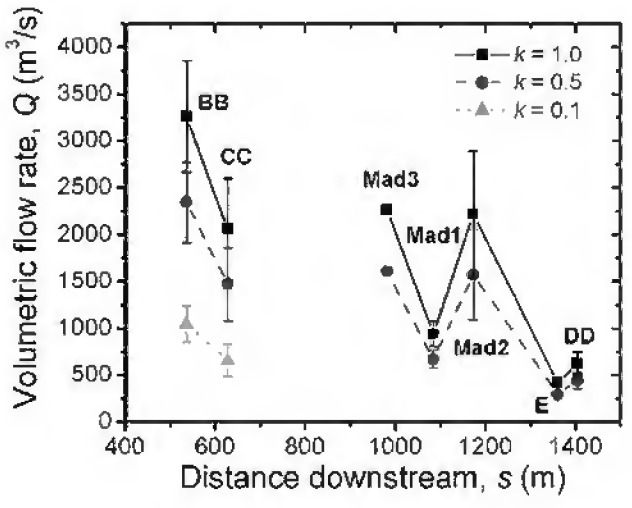

Figure 21. Variations in volumetric flow rate Q. The three lines correspond to three values for k used to determine average flow speed by superelevation (see text). The error bars result from the range of flow speeds obtained using different fits for the centerline radius of curvature of the channel.

Table 2. Values of Flow Resistance C

Cross Profile	C for $k = 1$[a]	C for $k = 0.5$[a]	C for $k = 0.1$[a]
BB	0.012–0.005	0.023–0.023	0.11–0.05
CC	0.047–0.026	0.092–0.050	0.46–0.25
Mad3	0.034	0.067	
Mad1	0.027–0.008	0.054–0.015	
Mad2	0.033–0.034	0.065–0.048	
E	0.044–0.005	0.088–0.009	
DD	0.048–0.019	0.096–0.037	
Average	0.035–0.013	0.069–0.019	0.29–0.14

[a] See text for discussion on superelevation constants k.

downstream should cause an increase in the General's slide flow speed downstream, which is physically unreasonable for near-constant h and inconsistent with the observed superelevation flow speeds.

[45] A second more promising possibility that may account for decreasing C downstream may be a decrease in channel roughness. One way to characterize channel roughness is to take the absolute value of the difference in elevation between the measured stream topography and the third-order polynomial fit of the channel elevation used to determine local channel slope. The resulting stream roughness (Figure 17) seems to vary nearly uniformly all the way downstream, with no significant decrease downstream. In addition, peaks in C for constant Q do not correlate with peaks in roughness. Decreasing streambed roughness thus probably does not account for the predicted decrease in C.

[46] A third influencing factor may be changes in flow direction associated with channel bends, which tend to increase resistance to flow [*Iverson*, 1997]. The biggest bends of the General's slide occur between Mad3 and Mad2 and between AA and CC (see Figure 2). However in both turns, C computed for a constant Q seems to decrease rather than increase (Figure 20).

[47] A fourth possibility that may account for decreasing C downstream is that the General's slide may have become more fluid downstream either by the deposition of entrained debris or the addition of surface runoff. Little deposition is observed between AA and DD (with the exception of a small region above Mad4); indeed, material was probably added to the debris flow in the upper (section 3.2.2) and lower tracks (see section 3.2.4). There is little preservation of hyperconcentrated and fluvial deposits that indicate that water content significantly increased in the General's slide on its way downstream.

[48] Thus values of C obtained from the simplifying assumption that Q is constant downstream do not seem to satisfy either physical arguments or geomorphologic indicators obtained at the General's slide. We therefore test if C values derived from superelevation flow speeds are more consistent with the observed geomorphology, thereby describing the dynamics of the flow. As before, four factors affect the overall changes in C downstream: (1) changes in flow speed, (2) changes in stream roughness, (3) changes in flow direction, and (4) changes in the fluidity of the debris flow.

[49] On the basis of our measurements, estimated flow speed decreases downstream (Figure 19). The resulting flow resistance should in theory decrease downstream as is expected in the case of a fully developed turbulent flow such as the General's slide. Results for C show a slight tendency to increase (Figure 20). Thus changes in C cannot be attributed to decreasing flow speeds.

[50] The influence of channel roughness also seems to be a minor contributor to changes in estimated flow resistance. As seen while analyzing the constant Q results, changes in C derived from superelevation flow speeds are not correlated with roughness (compare Figures 17 and 20). For example, the increase in resistance observed at CC and E occurs in one of the smoothest portions of the channel.

[51] The bends in the channel may play some role in influencing the measured flow resistance. For example, the biggest increase in C occurs following the second largest bend in the General's slide after BB. The value of C also increases after Mad1, the location of the largest bend in the channel.

[52] The flow resistance also tends to increase with the addition of material to the debris flow as well. The value of C increases in much of the upper track of the channel just below AA where the 1995 event eroded much of the preexisting channel. Similarly, C increases in the lower track below Mad1 where poorly consolidated material from the channel banks was entrained by the debris flow.

[53] Flow resistance also seems to decrease in regions where material is removed from the debris flow. The slight decrease in C predicted between CC and Mad3 is probably the result of debris deposited by the flow. The geomorphic evidence in this middle channel (section 3.2.3) indicates that the debris flow's speed probably slowed and spread out over an unconfined portion of the channel, resulting in some observed deposition of material.

[54] Changes in the flow resistance can also occur if water is removed or added to the debris flow. No geomorphic evidence indicates water loss along the channel except in the deposition fan. If anything, some water runoff was added to the debris flow by the small drainage network identified at the site, although its impact is not readily seen on the value of C.

[55] In summary, the predicted changes in C obtained by using superelevation flow speeds are consistent with the geomorphologic evidence for erosion and some deposition of material by the General's slide and the presence of bends in the channel. This is contrary to the results obtained using the assumption of constant volumetric flow rate Q, where little correlation appears to exist between the observed geomorphology and flow resistance. This analysis indicates that a better understanding of debris flow dynamics depends on obtaining debris flow speeds in addition to channel topography and flow thickness, rather than just on channel topography, flow thickness, and the assumption that Q is constant. Another approach providing similar insight into the dynamics of the flow requires solving simplified momentum equations using channel topography and flow thickness as constraints [e.g., *Baloga et al.*, 1995; *Bruno et al.*, 1996]. The current study also suggests

Table 3. Values of Flow Resistance C of Various Newtonian or Near-Newtonian Flows

Type	C	References
Water, smooth channel	0.0025	*Jeffreys* [1925]
Mudflow	0.002	*Plafker and Ericksen* [1978]
Pintubo-mudflow	0.0024	*Rodolfo et al.* [1996]
Sediment laden flow	0.005	*Komar* [1980]
Pintubo-hyperconcentrated flow	0.009–0.014	*Pierson et al.* [1996]
Mangatoetoenui-lahar	0.02–0.1	*Hodgson and Manville* [1999]
Pintubo-lahar	0.01–0.3	*Pierson et al.* [1996], *Rodolfo et al.* [1996]
Lahars	0.01–1.0	*Weir* [1982]
Debris flow	0.06–0.577	*Cruden and Lu* [1992], *Takahashi* [1980], *Johnson* [1984]
Wet landslide	0.184	*Cruden and Lu* [1992]

that the most important factors influencing flow resistance are the addition and removal of debris from a debris flow and the presence of bends.

6.2. Determining Flow Rheology

[56] The Chezy model has been used to examine the emplacement of lava flows [*Baloga et al.*, 1995], lahars [e.g., *Weir*, 1982], debris flows [e.g., *Takahashi*, 1980], and gravity-driven flows [*Bruno et al.*, 1996]. Comparisons between the empirical parameter C for the resistance to flow show that there are typical ranges for different flow processes, which reflect their rheology during emplacement. Broadly, increasing values of C correlate with increases in flow resistance, which relate in a complex manner to the effective flow viscosity and pore pressure. This suggests that the parameter C may be used as a diagnostic tool for determinations of the dynamics of emplaced landslides.

[57] We have made an initial search through the available literature to determine the necessary values to calculate C for pure water, debris flows, sediment-laden flows, and lahars. The search focused primarily on studies that included the variables in (3) necessary to determine C. This tended to significantly reduce availability of estimates for C since detailed slope and velocity are the parameters least well documented in mass movement studies.

[58] The values for C we computed for the General's slide range on average from 0.036 to 0.33, with our best guess ranging from 0.035 to 0.099 for $k = 0.5$. Comparison with Table 3 indicates that the main General's slide event had a rheology somewhere between a debris flow and a sediment-laden flow. The flow would be very much like a drier lahar with values of C near the top of the range obtained from Pinatubo lahars [*Pierson et al.*, 1996; *Rodolfo et al.*, 1996] or a wet debris flow, such as that seen in the lower section of the channel for a debris flow studied by *Cruden and Lu* [1992]. Very likely, the General's slide debris flow had significant water content. This interpretation was confirmed by eyewitness video of a nearby (~1 km away) debris flow that occurred near simultaneously to the main event at the General's slide. This analysis indicates that calculations of C can be used to determine to first order the rheology of flow features, thereby, greatly assisting in discriminating between similar looking deposits.

7. Conclusions and Planetary Implications

[59] These preliminary analyses at the General's slide debris flow demonstrate that understanding of the flow dynamics requires use of either flow speeds or simplified momentum equations [e.g., *Baloga et al.*, 1995; *Bruno et al.*, 1996] in addition to channel topography and flow thickness and that to first order, computations of resistance to flow provide constraints on the flow rheology. Using topographic data and Chezy-type models alone only partially constrains the dynamics of a flow. The use of additional terrestrial analogs for which detailed geomorphic observations, sedimentary analyses along the flow channel, and clast sizes are available is critical to validate the empirical values derived from Chezy-type models obtained when analyzing planetary data sets. The empirical values derived from Chezy-type models obtained when analyzing planetary data sets must be validated using terrestrial analogs where detailed geomorphic observations, sedimentary analyses along the flow channel, and clast sizes exist.

[60] Although mass movement processes are significant geomorphic agents on Earth and other terrestrial planets, studies have traditionally been limited to descriptions of surface morphology and measurements of lengths, widths, fall heights, and where stereo data were available, average thickness. High-resolution topography or imagery has not been available, severely restricting quantitative analysis of emplacement. Using Mars Global Surveyor (MGS) Mars Orbiter Camera (MOC) and Mars Orbiter Laser Altimeter (MOLA) data, it is now possible to obtain some accurate dimensional data over mass movement features. These data can be used to provide constraints on flow dynamics and flow rheology over deposits interpreted to be similar to terrestrial debris flows [e.g., *Carr*, 1996; *Malin and Edgett*, 2000]. Obtaining information about features such as those in Nirgal Vallis (<1 km long and tens of meters wide) remains difficult because of their small size relative to the MOLA shot spacing (>500 m) combined with the limited availability of high-resolution MOLA and MOC data. In addition, many of these proposed flows occur on steep crater and canyon walls [*Malin and Edgett*, 2000], making image geometry problematic. However, judicious use of the growing MOLA, MOC and the Thermal Emission Spectrometer (TES) data as well as comparison to appropriate terrestrial analogs provides the opportunity to examine to first order the behavior of proposed debris flows on Mars. In this way it is possible to empirically constrain their geomorphic origin and comment on any requirement for an interstitial fluid during their emplacement.

[61] Our field data show the complex processes involved in debris flows. In future work, this information will be linked to more sophisticated models that allow estimation of the amounts of fluid and solid [e.g., *Iverson*, 1997] in a debris flow, information that is of particular importance to understanding the size and evolution of water reservoirs on Mars. This work provides a foundation for analyzing existing MOC, MOLA, TES, and Viking data over proposed Martian debris flows.

[62] **Acknowledgments.** We are grateful to Scott Eaton, Alan Howard, Ben Morgan, and Jerry Wieczorek for discussion about the events at Graves Mill resulting from the 1995 storm. We thank Randall Lillard and his family for their interest in our work and access to the land around the General's slide. Andrew Johnson assisted with GPS data collection. Access to a sedimentary laboratory at the Smithsonian National Museum of Natural History was granted by Ian MacIntyre. We thank Bill Boykins and Thomas Jorstad for their assistance. We would also like to thank Lori Glaze and Steve Baloga for helpful discussions related to the modeling of flow processes.

References

Allen, R. M., Geology and mineral resources of Greene and Madison Counties, *Va. Div. Mines Res. Bull.*, *78*, 102 pp. , 1963.

Bagnold, R. A., Experiments in gravity-free dispersion of large solid spheres in a Newtonian fluid under shear, *Proc. R. Soc. London, Ser. A*, *225*, 49–63, 1954.

Baloga, S. M., P. D. Spudis, and J. E. Guest, The dynamics of rapidly emplaced terrestrial lava flows and implications for planetary lava flows, *J. Geophys. Res.*, *100*, 24,509–24,519, 1995.

Baloga, S. M., L. S. Glaze, J. A. Crisp, and S. A. Stockman, New statistics for estimating bulk rheology of active lava flows: Pu'u O'o examples, *J. Geophys. Res.*, *103*, 5133–5142, 1998.

Blair, T. C., and J. G. McPherson, Grain-size and textural classification of coarse sedimentary particles, *J. Sed. Res.*, *69*, 6–19, 1999.

Bovis, M. J., and M. Jakob, The role of debris supply conditions in predicting debris flow activity, *Earth Surf. Process. Landforms*, *24*, 1039–1054, 1999.

Bruno, B. C., S. M. Baloga, and G. J. Taylor, Modeling gravity-driven flows on an inclined plane, *J. Geophys. Res.*, *101*, 11,565–11,577, 1996.

Carr, M. H., *Water on Mars*, Oxford Univ. Press, 229 pp., New York, 1996.

Chen, C., Comprehensive review of debris flow modeling concepts in Japan, in *Debris Flows/Avalanches: Process, Recognition, and Mitigation*, edited by J. E. Costa and G. F. Wieczorek, *Rev. Eng. Geol.*, *7*, 13–29, 1987.

Costa, J. E., Physical geomorphology of debris flows, in *Developments and Application of Geomorphology*, edited by J. E. Costa and P. J. Fleisher, pp. 268–312, Springer-Verlag, New York, 1984.

Cruden, D. M., and Z. Y. Lu, The rockslide and debris flow from Mount Cayley, B.C., in June 1984, *Can. Geotech. J.*, *29*, 614–626, 1992.

Hodgson, K. A., and V. R. Manville, Sedimentology and flow behavior of a rain-triggered lahar, Mangatoetoenui stream, Ruapehu volcano, New Zealand, *Geol. Soc. Am. Bull.*, *5*, 743–754, 1999.

Iverson, R. M., The physics of debris flows, *Rev. Geophys.*, *35*, 245–297, 1997.

Jeffreys, H., The flow of water in an inclined channel of rectangular section, *Philos. Mag.*, *49*, 793–807, 1925.

Johnson, A. M., *Physical Processes in Geology*, 557 pp., W. H. Freeman, New York, 1970.

Johnson, A. M., Debris flow, in *Slope Instability*, edited by D. Brunsden and D. B. Prior, pp. 257–361, John Wiley, New York, 1984.

Kochel, R. C., and R. A. Johnston, Geomorphology and sedimentology of humid-temperate alluvial fans, central Virginia, in *Sedimentology of Gravels and Conglomerates*, edited by E. H. Koster and R. J. Steele, *Mem. Can. Soc. Petrol. Geol.*, *10*, 109–122, 1984.

Komar, P. D., Modes of sediment transport in channelized water flows with ramifications to the erosion of Martian outflow channels, *Icarus*, *42*, 317–329, 1980.

Major, J. J., and R. M. Iverson, Debris flow deposition: Effects of pore fluid pressure and friction concentrated at flow margins, *Geol. Soc. Am. Bull.*, *111*, 1424–1434, 1999.

Malin, M. C., and K. S. Edgett, Evidence for recent groundwater seepage and surface runoff on Mars, *Science*, *288*, 2330–2335, 2000.

Mills, H. H., Long-term episodic deposition on mountain foot-slopes in the Blue Ridge province of North Carolina: Evidence from relative age dating, *Southeastern Geol.*, *23*, 123–128, 1982.

Mizuyama, T., and S. Uehara, Debris flow in steep slope channels, *Civ. Eng. J. Jpn.*, *23*(5), 243–248, 1981.

Morgan, B. A., G. F. Weiczorek, and R. H. Campbell, Debris-flow hazards in the areas affected by the June 27, 1995, storm in Madison county, Virginia, *U.S. Geol. Surv. Open File Rep., 97-438*, 1–15, 1997.

Paterson, W. S. B., *Physics of Glaciers*, 250 pp., Pergamon, New York, 1969.

Pierson, T. C., A. S. Daag, P. J. D. Reyes, M. T. M. Regalado, R. U. Solidum, and B. S. Tubianosa, Flow and deposition of posteruption hot lahars on the east side of Mount Pinatubo, July–October 1991, in *Fire and Mud: Eruptions and Lahars of Mount Pinatubo, Philippines*, edited by C. G. Newhall and R. S. Punongbayan, Univ. of Wash. Press, Seattle, 1996.

Plafker, G., and G. E. Ericksen, Nevados Hauscaran avalanches, Peru, in *Rockslides and Avalanches,* part 1, *Natural Phenomena,* edited by B. Voight, pp. 277–314, Elsevier Sci., New York, 1978.

Rodolfo, K. S., J. V. Umbal, R. A. Alonso, C. T. Remotigue, M. A. Paldo-Melosantos, J. H. G. Salvador, D. Evangelista, and Y. Miller, Two years of lahars on the western flank of Mount Pinatubo: Initiation, flow processes, deposits, and attendant geomorphic and hydraulic changes, in *Fire and Mud: Eruptions and Lahars of Mount Pinatubo, Philippines*, edited by C. G. Newhall and R. S. Punongbayan, Univ. of Wash. Press, Seattle, 1996.

Savage, S. B., and K. Hutter, The motion of a finite mass of granular material down a rough incline, *J. Fluid Mech.*, *199*, 177–215, 1984.

Simpson, J. E., *Gravity Currents in the Environment and the Laboratory*, 2nd ed., 244 pp., Cambridge Univ. Press, New York, 1997.

Sohn, Y. K., Coarse-grained debris-flow deposits in the Miocene fan deltas, SE Korea: A scaling analysis, *Sed. Geol.*, *130*, 45–64, 2000.

Takahashi, T., Debris flows on prismatic open channel, *J. Hydraul. Div. Am. Soc. Civ. Eng.*, *106*(HY3), 381–396, 1980.

Takahashi, T., Debris flow, *Annu. Rev. Fluid Mech.*, *13*, 57–77, 1981.

Weir, G. J., Kinematic wave theory for Ruapehu lahars, *N. Z. J. Sci.*, *25*, 197–203, 1982.

White, F., *Fluid Mechanics*, McGraw-Hill, New York, 1993.

Wieczorek, G. F., B. A. Morgan, R. H. Campbell, R. C. Orndorff, W. C. Burton, C. S. Southworth, and J. A. Smith, Preliminary inventory of debris-flow and flooding effects on the June 27, 1995 storm in Madison County, Virginia showing time sequence of positions and storm-cell center, *U.S. Geol. Surv. Open File Rep., 96-13*, 1–8, 1996.

Wieczorek, G. F., B. A. Morgan, and R. H. Campbell, Debris-flow hazards in the Blue Ridge of central Virginia, *Environ. Eng. Geosci.*, *6*(1), 3–23, 2000.

M. H. Bulmer, Joint Center for Earth Systems Technology, University of Maryland, Baltimore County, 1000 Hilltop Circle, Baltimore, MD 21250, USA. (mbulmer@jcet.umbc.edu)

O. S. Barnouin-Jha, Johns Hopkins University Applied Physics Laboratory, Laurel, MD 20723-6099, USA.

M. N. Peitersen, Proxemy Research, 20528 Farcroft Lane, Laytonsville, MD 20882, USA.

Mary Bourke, School of Geography and the Environment, University of Oxford, Mansfield Road, Oxford OX1 3TB, UK.

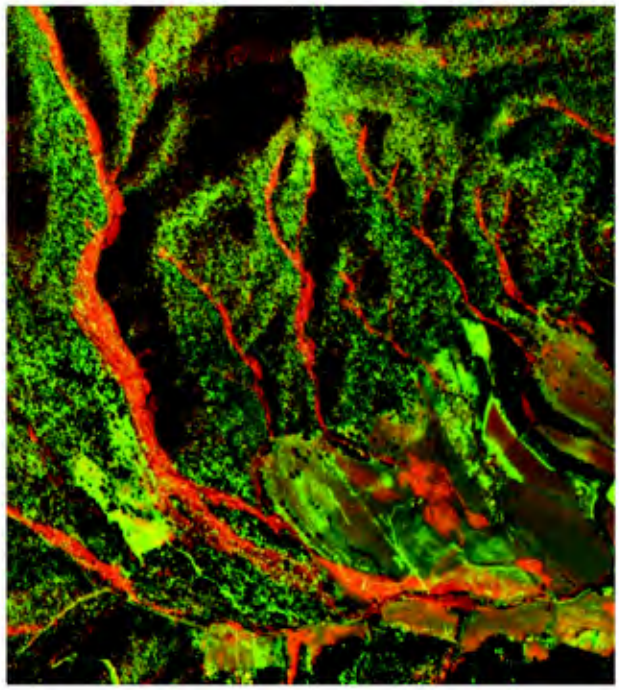

Figure 3. Anaglyph of 1:18,000 scale air photographs from April 1991 (right eye) and March 1997 (left eye) showing the landscape change between these dates resulting from the storm in July 1995 (orange coloration). The image in the left eye shows the area around the General's slide two years after the 1995 storm. Compare this to the image in the right eye that shows the area of the General's slide as it was in 1991. The channel was tree covered and is shown by the blue colored transect lines seen in Figure 3. Comparison of the debris apron with Figure 2 taken August 1995 shows that much of the material in the depositional zone has been removed by heavy machinery to restore the productivity of the field.